Measurement of optical scattering properties using line-field confocal optical coherence tomography (LC-OCT)

Léna Waszczuk, Jonas Ogien, Frederic Pain, Arnaud Dubois

Measurement of optical scattering properties using line-field confocal optical coherence tomography (LC-OCT)

Léna Waszczuk[a,b], Jonas Ogien[b], Frédéric Pain[a], and Arnaud Dubois[a,b]

[a]Université Paris-Saclay, Institut d'Optique Graduate School, CNRS, Laboratoire Charles Fabry, Palaiseau 91127, France
[b]DAMAE Medical, Paris 75013, France

ABSTRACT

Line-field confocal optical coherence tomography (LC-OCT) is an imaging technique that combines the principles of time-domain OCT and reflectance confocal microscopy (RCM). LC-OCT was designed to generate three-dimensional (3D) morphological images of the skin, *in vivo*, with a spatial resolution of ~ 1 µm. As in OCT and RCM, LC-OCT image contrast originates from the backscattering of incident light by the sample microstructures, which is determined by the optical scattering properties of the sample, namely the scattering coefficient μ_s and the scattering anisotropy parameter g. When imaging biological tissues, these properties can provide insight into tissue organization and structure, and could be used for quantitative tissue characterization *in vivo*. We present a method for obtaining spatially-resolved measurements of optical scattering parameters from LC-OCT images. Our approach is based on a calibration using a test sample with known optical scattering properties and on the application of a theoretical model previously developed for focus-tracking mode OCT and RCM. Assuming a single-scattering regime, this model allows to derive the optical scattering parameters μ_s and g from the intensity depth profiles acquired by LC-OCT. Spatially-resolved measurements are achieved by dividing the 3D LC-OCT image into "macro-voxels" and analyzing the different sample layers separately, leading to 3D distributions of μ_s and g. This method was experimentally tested against integrating spheres and collimated transmission measurements and validated on a set of mono- and bi-layered scattering phantoms.

Keywords: line-field confocal optical coherence tomography, optical coherence tomography, reflectance confocal microscopy, optical properties, scattering

1. INTRODUCTION

Line-field confocal optical coherence tomography (LC-OCT) is a recently introduced imaging technique which provides two-dimensional (2D) and three-dimensional (3D) images of semi-transparent samples with a quasi-isotropic resolution of ~ 1 µm.[1] Up to now, LC-OCT has been applied in the field of dermatology[2–5] where it provides *in vivo* images of the superficial layers of the skin down to 500 µm depth. Images are generated with a cellular resolution similar to the one of histology, while being non-invasive.

LC-OCT images provide structural information, which arises from the backscattering of light by microstructures within the analyzed sample. Backscattering can be characterized by optical properties including the absorption coefficient μ_a, the scattering coefficient μ_s and the scattering anisotropy parameter g. The scattering properties μ_s and g are determined by structural parameters of the analyzed samples, such as size, shape, density and refractive index of tissue light scatterers. Extracting the scattering properties from LC-OCT images could provide LC-OCT with further quantitative information and serve as a metric to monitor structural changes occurring in tissues.

Optical measurement techniques using integrating spheres and collimated transmission allow extraction of the scattering properties of *ex vivo* tissues. However, few techniques allow *in vivo* measurements of the scattering properties μ_s and g. In this paper, we describe a method to extract μ_s and g *in vivo* from 3D LC-OCT images. The approach was developed on mono- and bi-layered test samples and validated against integrating spheres and collimated transmission measurements. Additionally, we introduce spatially-revolved measurements of μ_s and g, obtained by convolving the 3D LC-OCT image with a region of interest (ROI) of macroscopic size.

Further author information: (Send correspondence to Léna Waszczuk)
Léna Waszczuk: E-mail: lena.waszczuk@universite-paris-saclay.fr

2. MATERIALS AND METHODS

2.1 Phantoms

Test samples with various optical properties, also called phantoms, were made. These phantoms are composed of a polydimethylsiloxane (PDMS) matrix in which scattering particles were included. Particles of various materials were chosen as scattering material: titanium dioxide (TiO_2), zinc oxide (ZnO) and silicon dioxide (SiO_2) micro- and nano-powders. Six monolayered phantoms were fabricated, with scattering properties close to those of biological tissues.[6] Additionally, all phantoms have negligible absorption compared to scattering in the near infrared range, similarly to most biological tissues. We also designed bilayered phantoms with distinct optical properties in each layer. Top layer thickness down to 100 µm was achieved, allowing to image both layers within the 500 µm depth scan range of the LC-OCT device.

2.2 LC-OCT device

The LC-OCT device used in this work was previously described in detail in the literature.[1,7,8] The principle of LC-OCT relies on the combination of two optical imaging techniques: time-domain optical coherence tomography (TD-OCT) and reflectance confocal microscopy (RCM), using line illumination with a broadband laser centered around 800 nm and detection with a line camera. The LC-OCT device is capable of generating both 2D vertical images (B-scan, $x \times z$) and horizontal images ($x \times y$). By combining the depth and lateral scans, 3D images can also be obtained, covering a field of view of 1.2 mm × 0.5 mm × 0.5 mm ($x \times y \times z$) with a quasi-isotropic resolution of $\sim$ 1 µm.

2.3 Integrating spheres and collimated transmission measurements

Measurements of μ_s and g were performed using a set-up with two integrating spheres. Light from a high-power broadband Xenon light source was guided to one of the two spheres and collimated into a 6-mm diameter beam. The phantom was placed between the two spheres. Diffuse reflected and transmitted light was collected by a spectrometer. Collimated transmission measurement was carried out using a 785 nm laser. The unscattered light was selected using a pinhole placed one meter behind the phantom and collected using the same fiber and spectrometer as for the diffuse reflectance and transmittance measurements. All measurements were subtracted from noise and normalized with respect to blank measurements with no sample. The optical properties μ_s and g were computed at 785 nm using the inverse adding doubling (IAD) algorithm by S. L. Jacques and S. Prahl.[9]

2.4 Extraction of μ_s and g from 3D LC-OCT images

For each phantom, a 3D LC-OCT image is acquired and the mean intensity depth profile $R(z)$ is computed by averaging all A-scans within the 3D image. In the assumption of a single-scattering regime (which can be considered valid when $\mu_s z \leq 1$) and a homogeneous sample, $R(z)$ follows an exponential decay with depth modeled by the Beer-Lambert law:

$$R(z) = \rho \, exp(-2\mu z)$$

ρ and μ are defined as the backscattering coefficient and attenuation coefficient. ρ and μ are experimental observables, determined both by the sample optical properties and the imaging device characteristics including the numerical aperture (NA) of the microscope objective and the temporal coherence of the light source. ρ and μ are extracted by applying a least square linear regression on $log\, R(z)$, as shown in Fig 1(b). At this point, a calibration step is required to convert ρ from gray levels into reflectance units. This calibration is achieved using one of the fabricated phantoms whose scattering properties were determined by integrating spheres and collimated transmission.

ρ and μ are then mapped to the optical properties μ_s and g using a model previously introduced by S. L. Jacques *et al.*[10] This model, developed for OCT in focus-tracking mode and RCM, is based on Monte-Carlo simulations. The model was developed and validated on phantoms of known optical properties[11] and later applied to the characterization of optical properties of various biological tissues including mice brain, skin, liver, muscle,[12] bird skull[13] and human retina.[14]

For bilayered phantoms, spatially-resolved measurements in the Z direction were obtained by applying a linear regression separately on each layer. Attenuation due to propagation in the top layer was taken into

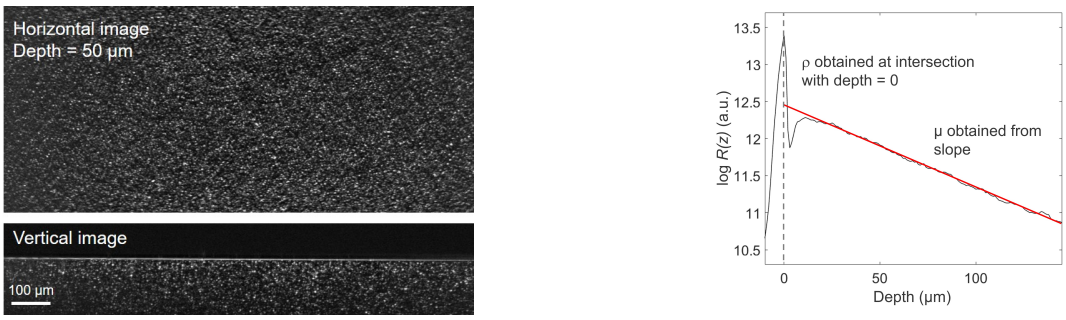

(a) (b)

Figure 1: (a) LC-OCT images (horizontal and vertical views) of a phantom made of PDMS and TiO_2 particles and (b) averaged intensity profile $R(z)$ in the 3D LC-OCT image as a function of depth, in logarithmic scale. A linear regression is applied on the intensity profile to obtain the measurement of the pair of observables μ and ρ.

account to determine optical properties of the bottom layer. In the lateral plane ($x \times y$), spatially-resolved measurements of the optical properties were obtained by convolving the 3D LC-OCT image (*i.e.* each horizontal image constituting the 3D image) with a 150 µm^2 ROI. Each A-scan of the resulting image corresponds to the intensity profile averaged in a ROI centered on the position of this A-scan in the original 3D LC-OCT image. Values of μ_s and g can then be extracted from each A-scan to provide a mapping of the optical properties μ_s and g over the lateral ($x \times y$) LC-OCT field of view, with macroscopic resolution. By combining Z- and XY-resolved measurements, measurements of μ_s and g within macroscopic voxels could be obtained.

3. RESULTS AND DISCUSSION

Comparisons of μ_s and g values of monolayered phantoms obtained from LC-OCT mean intensity depth profiles and integrating spheres and collimated transmission measurements are given in Figs 2 and 3. For all six phantoms, a good agreement is obtained between the LC-OCT measurements and the integrating spheres and collimated transmission measurements.

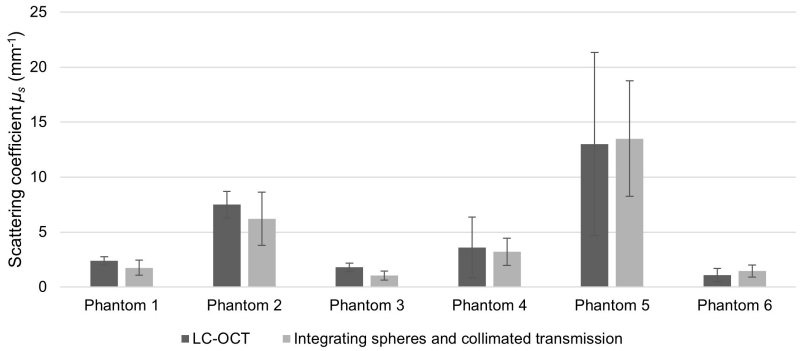

Figure 2: Comparison of μ_s values obtained from LC-OCT and integrating spheres and collimated transmission measurements on monolayered phantoms.

Our method was further validated on bilayered phantoms (see Fig 4). For each layer, LC-OCT provides values of g that are in very good agreement with the integrating spheres and collimated transmission measurements, despite very different g values in each layer. Results on μ_s are also consistent, despite a slight underestimation of the μ_s value for the top layer of bilayered phantom n°1 and the bottom layer of bilayered phantom n°2. The top layer of bilayered phantom n°1 was fabricated from the same PDMS/SiO_2 mixture as the monolayered phantom 5 of Fig. 2. Since the resulting layer was very thin ($\leq$ 100 µm) and fragile, we were not able to characterize its values of μ_s and g using integrating spheres and collimated transmission measurements and assumed they were identical as monolayered phantom 5, which could be a limitation to our approach. More investigations are needed

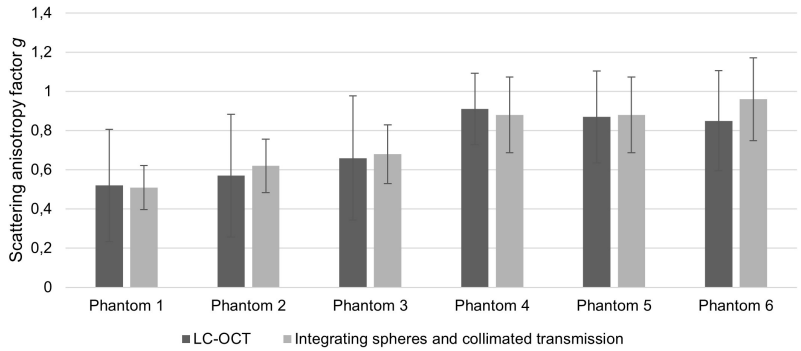

Figure 3: Comparison of g values obtained from LC-OCT and integrating spheres and collimated transmission measurements on monolayered phantoms.

to understand this issue. In the bottom layer of bilayered phantom n°2, underestimation of μ_s could be caused by a potential a contribution from multiple scattering, due to his high value of μ_s. Nevertheless, the values of μ_s remain close to the values obtained using integrating spheres and collimated transmission, considering the extent of the error bars shown on the graphs.

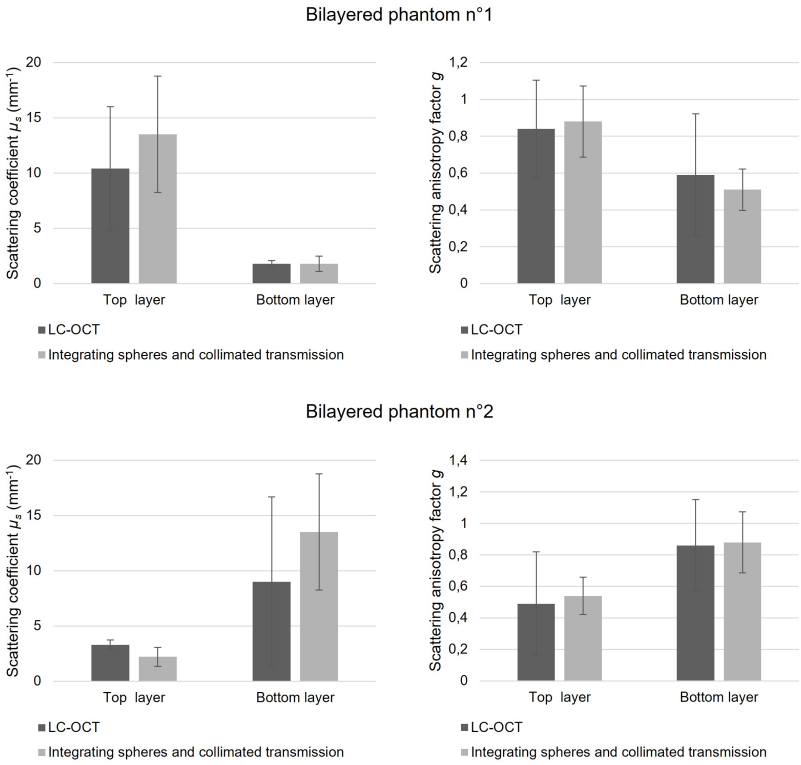

Figure 4: Comparison of μ_s and g values obtained from LC-OCT and integrating spheres and collimated transmission measurements on two different bilayered phantoms.

Finally, preliminary results of the spatially-resolved measurement of μ_s and g are shown in Fig 5. Two phantoms with different optical properties (monolayered phantoms 1 and 5) were placed side by side within the field of view of a 3D LC-OCT image. The spatial distributions of μ_s and g show two very distinct areas, corresponding to each of the two phantoms. For each area, values of μ_s and g are consistent with the expected values given in Figs 2 and 3 despite slight heterogeneities at the macro-pixel scale. Further work is still needed to

validate this spatially-resolved approach, using for example samples with sharper variations in optical properties at the macro-pixel scale.

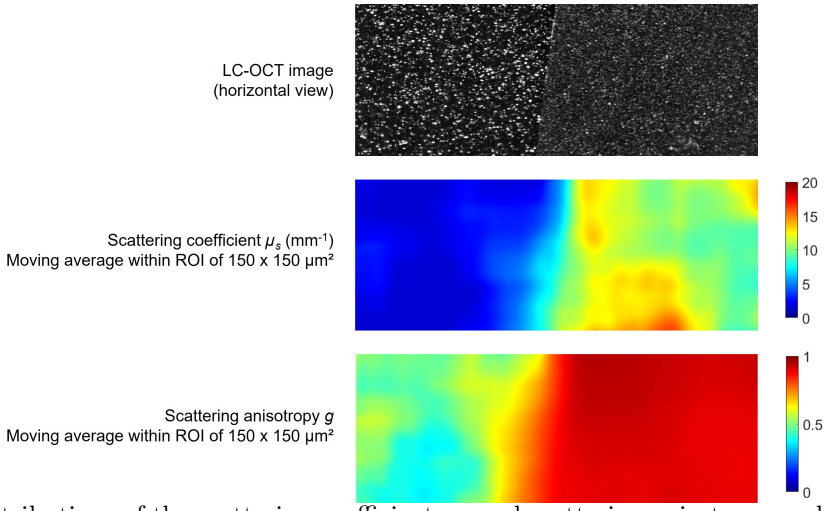

Figure 5: Spatial distributions of the scattering coefficient μ_s and scattering anisotropy g obtained from a single 3D LC-OCT image of two side-by-side phantoms of different optical properties.

4. CONCLUSION

This paper reports on a method to measure the optical scattering parameters μ_s and g of mono- and bi-layered phantoms from 3D LC-OCT images. The method relies on a calibration using a test sample with known optical scattering properties and on the application of a theoretical model previously developed for focus-tracking mode OCT and RCM,[14] applied to the LC-OCT intensity depth profile. The approach was tested on phantoms with various optical properties, and compared to a method commonly used in the literature based on integrating spheres and collimated transmission. Results obtained with both methods are in good agreement, suggesting that LC-OCT is a relevant tool for the quantification of optical properties.

For bilayered phantoms, the optical properties of both layers can be extracted from a single 3D LC-OCT image, unlike integrating spheres where both layers must be analyzed separately. Finally, we introduced a method to obtain spatial distributions of the two optical parameters μ_s and g within a 3D LC-OCT image. This approach still needs to be tested on heterogeneous samples to better evaluate its potential. Although of low resolution compared to the cellular resolution of LC-OCT, the spatially-resolved measurement would provide LC-OCT with a tool to quantify scattering properties of the imaged sample at macroscopic scale, complementary to the qualitative information provided by the high-resolution image.

The method presented in this paper needs to be further investigated for application to biological tissues. Eventually, the method could be used as a metric to quantify changes in biological tissues *in vivo*, or even to observe variations from one area to another within a 3D LC-OCT image.

REFERENCES

[1] Ogien, J., Daures, A., Cazalas, M., Perrot, J. L., and Dubois, A., "Line-field confocal optical coherence tomography for three-dimensional skin imaging," *Frontiers of Optoelectronics* **13**(4), 381–392 (2020).

[2] Monnier, J., Tognetti, L., Miyamoto, M., Suppa, M., Cinotti, E., Fontaine, M., Perez, J., Orte Cano, C., Yélamos, O., Puig, S., Dubois, A., Rubegni, P., del Marmol, V., Malvehy, J., and Perrot, J. L., "In vivo characterization of healthy human skin with a novel, non-invasive imaging technique: line-field confocal optical coherence tomography," *Journal of the European Academy of Dermatology and Venereology* **34**(12), 2914–2921 (2020).

[3] Dejonckheere, G., Suppa, M., del Marmol, V., Meyer, T., and Stockfleth, E., "The actinic dysplasia syndrome – diagnostic approaches defining a new concept in field carcinogenesis with multiple cSCC," *Journal of the European Academy of Dermatology and Venereology* **33**(S8), 16–20 (2019).

[4] Suppa, M., Fontaine, M., Dejonckheere, G., Cinotti, E., Yélamos, O., Diet, G., Tognetti, L., Miyamoto, M., Orte Cano, C., Perez-Anker, J., Panagiotou, V., Trepant, A., Monnier, J., Berot, V., Puig, S., Rubegni, P., Malvehy, J., Perrot, J., and Marmol, V., "Line-field confocal optical coherence tomography of basal cell carcinoma: a descriptive study," *Journal of the European Academy of Dermatology and Venereology* **35**(5), 1099–1110 (2021).

[5] Ruini, C., Schuh, S., Gust, C., Kendziora, B., Frommherz, L., French, L., Hartmann, D., Welzel, J., and Sattler, E., "Line-field optical coherence tomography: In vivo diagnosis of basal cell carcinoma subtypes compared to histopathology," *Clinical and Experimental Dermatology* , 0–3 (2021).

[6] Jacques, S. L., "Optical properties of biological tissues: A review," *Physics in Medicine and Biology* **58**(11) (2013).

[7] Dubois, A., Levecq, O., Azimani, H., Siret, D., Barut, A., Suppa, M., del Marmol, V., Malvehy, J., Cinotti, E., Rubegni, P., and Perrot, J.-L., "Line-field confocal optical coherence tomography for high-resolution noninvasive imaging of skin tumors," *Journal of Biomedical Optics* **23**(10), 1 (2018).

[8] Ogien, J., Levecq, O., Azimani, H., and Dubois, A., "Dual-mode line-field confocal optical coherence tomography for ultrahigh-resolution vertical and horizontal section imaging of human skin in vivo," *Biomedical Optics Express* **11**(3), 1327 (2020).

[9] Prahl, S., "Optical property measurements using the inverse adding-doubling program," *Oregon Medical Laser Center, St. Vincent Hospital* **2197**(January) (1995).

[10] Jacques, S. L., "Confocal Laser Scanning Microscopy Using Scattering as the Contrast Mechanism," *Handbook of Coherent-Domain Optical Methods* **1-2**, v–xiv (2013).

[11] Samatham, R. and Jacques, S. L., "Determine scattering coefficient and anisotropy of scattering of tissue phantoms using reflectance-mode confocal microscopy," *Biomedical Applications of Light Scattering III* **7187**(February), 718711 (2009).

[12] Choudhury, N. and Jacques, S. L., "Extracting scattering coefficient and anisotropy factor of tissue using optical coherence tomography," *Optical Interactions with Tissue and Cells XXIII* **8221**, 822111 (2012).

[13] Abi-Haidar, D. and Olivier, T., "Confocal reflectance and two-photon microscopy studies of a songbird skull for preparation of transcranial imaging," *Journal of Biomedical Optics* **14**(3), 034038 (2009).

[14] Jacques, S. L., Samatham, R., Choudhury, N., Fu, Y., and Levitz, D., "Measuring tissue optical properties in vivo using reflectance-mode confocal microscopy and OCT," *Biomedical Applications of Light Scattering II* **6864**(68640), 68640B (2008).